RSC Advances

PAPER

View Article Online
View Journal | View Issue

Cite this: *RSC Adv.*, 2021, **11**, 27193

Metal-centered monocyclic carbon wheel clusters with record coordination numbers in planar species†

Xiao-Qin Lu, Hai-Gang Lu* and Si-Dian Li*

The highest coordination number identified to date in planar species is CN = 10 in metal-centered monocyclic boron wheel clusters D_{10h} M©B_{10}^- (M = Ta and Nb) (Galeev *et. al.*, *Angew. Chem. Int. Ed.*, 2012, **51**, 2101). Extensive global minimum searches and first-principles theory calculations performed herein indicate that the experimentally observed LaC_{13}^+ and LaC_{14}^+ possess the well-defined global minima of perfect metal-centered monocyclic carbon wheel D_{13h} La©C_{13}^+ (**1**) ($1A_1'$) and slightly off-centered C_{2v} La©C_{14}^+ (**4**) ($^1A_1$) with record coordination numbers of CN = 13 and 11 in planar structures, respectively, further pushing the boundary of our understanding of chemical structures and bonding. Detailed molecular orbital, nucleus-independent chemical shift, and ring current analyses indicate that D_{13h} La©C_{13}^+ (**1**) is σ + π dually aromatic in nature, with 14 totally delocalized in-plane σ electrons and 14 totally delocalized out-of-plane π electrons each matching the $4N + 2$ aromatic rule ($N_\sigma = N_\pi = 3$). Similar σ + π dually aromatic metal-centered monocyclic wheel clusters D_{13h} Ca©C_{13} (**2**), C_{13v} Ac©C_{13}^+ (**3**), C_{2v} Y©$B_6C_6^+$ (**5**), and C_{2v} Sc©B_5C_6 (**6**) have also been obtained with CN = 13, 13, 12, and 11, respectively. The results obtained in this work effectively enrich the chemical structures and bonding patterns of planar hypercoordinated complexes.

Received 12th July 2021
Accepted 3rd August 2021

DOI: 10.1039/d1ra05367a

rsc.li/rsc-advances

1. Introduction

Searching for the maximum coordination number in planar species has fascinated chemists for many years and continuously pushed the boundary of our understanding of chemical structures and bonding.[1,2] The central atom and periphery atoms around it in the ligand in stable planar hypercoordinated structures must match both geometrically and electronically, *i.e.*, they must have the right atomic sizes and electronic configurations. The experimentally observed boron-centered monocyclic boron wheel clusters D_{7h} B©B_7^{2-} and D_{8h} B©B_8^- are good examples in which the central B atoms have the coordination numbers of CN = 7 and 8, respectively.[3] These boron cluster monoanions prove to be σ + π dually aromatic in nature with six delocalized σ and six delocalized π electrons (6 σ + 6 π) each conforming to the $4N + 2$ aromatic rule ($N_\sigma = N_\pi = 1$). Based on the double aromaticity requirement in bare boron wheel clusters, a general electronic design principle $x + n + k = 12$ or 16 was developed for metal-centered monocyclic boron wheel clusters M©B_n^{k-} by the groups of Wang and Boldyrev,[1,4–6] where x stands for the formal valence of the metal center M. This design principle has been successfully applied to the experimentally characterized octacoordinated D_{8h} Co©B_8^- with CN = 8,[5] nonacoordianted D_{9h} Ru©B_9^-, D_{9h} Rh©B_9^-, and D_{9h} Ir©B_9^- with CN = 9,[7,8] and, finally, to the decacoordinated D_{10h} Ta©B_{10}^- and D_{10h} Nb©B_{10}^- with CN = 10 which has proven to be the highest coordination number in planar species observed to date.[1,2]

However, planar hypercoordination chemistry may go well beyond metal-centered monocyclic boron wheel clusters. The recent experimental characterization of perfect planar D_{9h} C_{18} by atom manipulations and high-resolution atomic force microscopy[9] inspires us to coordinate transition metal centers with bare cyclo[*n*]carbon ring-like clusters (C_n, $n \geq 11$) to form metal-centered monocyclic carbon wheel complexes M©C_n^{k+}. Very recently, the electronic properties of metal-carbon ring complexes such as Li@C_{18} and MC_{16} have been reported.[10,11] Carbon ([He]$2s^22p^2$) is known to be effective ligand to various transition metals with a smaller covalent radius than boron ([He]$2s^22p^1$), while group IIIB metals La, Y, and Sc with the valence electronic configurations of (n-1)d^1ns^2 possess the largest covalent radii in the periodic table.[12] Metal-centered monocyclic carbon wheel clusters M©C_n^{k+} (M = La, Y, Sc) are thus possible to have even higher coordination numbers than their boron counterparts M©B_n^{k-}. In fact, two families of LaC_n^+ monocations (n = 12–40) were observed in mobility measurements as early as in 1994, with a La atom inserted into the carbon ring for even-numbered clusters or attached to the inside or outside of the carbon ring for odd-numbered

Nanocluster Laboratory, Institute of Molecular Science, Shanxi University, Taiyuan 030006, China. E-mail: luhg@sxu.edu.cn; lisidian@sxu.edu.cn

† Electronic supplementary information (ESI) available. See DOI: 10.1039/d1ra05367a

clusters.[13] More detailed mass spectra were reported late on LaC_n^+ in which LaC_{13}^+ appeared to be a prominent species with the La center most likely attached inside a C_{13} ring (ring Ib), while LaC_{14}^+ was the only LaC_{2n}^+ cluster with even number of C atoms for which ring Ib structure had a higher mass intensity than its competing isomer with a La atom inserted into a C_{14} ring (ring Ia).[14] Similar prominent mass peaks were also observed for YC_{13}^+, CeC_{13}^+, and ScC_{13}^+.[15] Early density functional theory (DFT) calculations indicated that the most stable isomer of LaC_{13}^+ possessed a nearly-cumulenic structure with the La atom located at the center of the carbon ring.[16,17] However, the unique role these experimentally observed LaC_n^+ species ($n = 13$, 14) play in planar hypercoordination chemistry has largely omitted in previous investigations and their accurate geometrical and electronic structures and detailed La–C coordination bonding patterns remain to be fully evaluated using the state-of-the-art theoretical approaches to interpret their behaviors observed in experiments.

Detailed first-principles theory calculations performed in this work indicate that the experimentally observed $La©C_{13}^+$ (**1**) with a perfect D_{13h} symmetry and slightly off-centered $La©C_{14}^+$ (**4**) with a C_{2v} geometry achieve the record coordination numbers of CN = 13 and 11 in planar species reported to date. The enhanced stability of $La©C_{13}^+$ (**1**) originates from its σ + π dual aromaticity with 14 delocalized σ electrons and 14 delocalized π electrons (14 σ + 14 π) each matching the $4N + 2$ aromatic rule ($N_\sigma = N_\pi = 3$). σ + π dually aromatic D_{13h} $Ca©C_{13}$ (**2**), C_{13v} $Ac©C_{13}^+$ (**3**), C_{2v} $Y©B_6C_6^+$ (**5**), and C_{2v} $Sc©B_5C_6$ (**6**) have also been obtained at first-principles theory level with CN = 13, 13, 12, and 11, respectively. The highly stable $La©C_{13}^+$ (**1**) is found to behave like a super-hydrogen monocation (H^+) in its substituted complex compounds.

2. Theoretical procedure

Extensive global-minimum (GM) searches were performed on LaC_{13}^+, LaC_{14}^+, CaC_{13}, AcC_{13}^+, $YB_6C_6^+$, ScB_5C_6, and $CeC_{13}^{+/2+}$ using the TGmin2 code[18] at DFT level based on the constraint basin-hopping algorithm.[19] In total, more than 1000 stationary points with different spin multiplicities were probed for each species at PBE/DZVP level using the CP2K program.[20,21] Low-lying isomers were then fully optimized at the M06-2X and PBE0 level,[22,23] with the 6-311+G(d,p) basis sets for C, B, N, Ca, and Sc[24] and Stuttgart relativistic small-core pseudopotentials for La, Y, Ce, and Ac,[25,26] using the Gaussian-16 program suite.[27] Frequency analyses were performed to make sure all the optimized structures are true minima of the systems. Relative energies for the five lowest-lying isomers were further refined using the more accurate coupled cluster method with triple excitations CCSD(T)[28–30] implemented in Molpro[31] with the basis set of cc-pVTZ for C, B, N, Ca, and Sc and the Stuttgart small-core pseudopotential for La, Y, and Ac. The optimized GM structures are summarized in Fig. 1 and more alternative isomers tabulated in Fig. S1–S6.† Natural bonding orbital (NBO) analyses were performed using the NBO 6.0 program.[32] Born–Oppenheimer molecular dynamics (BOMD) simulations were performed on LaC_{13}^+ (**1**) for 30 ps using the CP2K software suite at 300, 800, and 1000 K.[21] The anisotropy of the current-induced density (ACID)[33] analyses were performed using the ACID code, with the ring-current maps generated using POV-Ray 3.7.[34] The iso-chemical shielding surfaces (ICSSs)[35,36] were generated with the Multiwfn 3.8 code.[37] The UV-vis spectra were simulated using the time-dependent TD-DFT-M06-2X approach.[38]

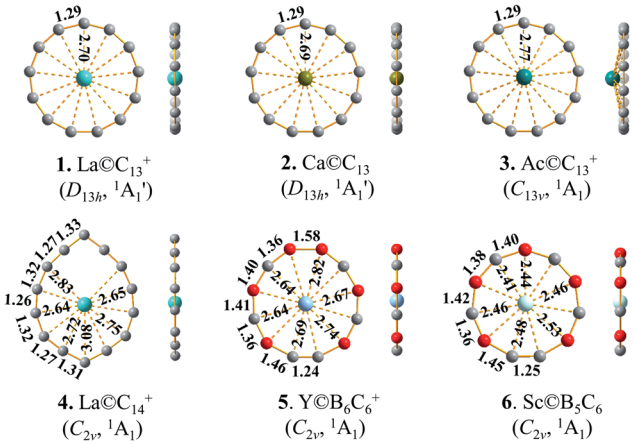

Fig. 1 Top and side views of the optimized $La©C_{13}^+$ (**1**), $Ca©C_{13}$ (**2**), $Ac©C_{13}^+$ (**3**), $La©C_{14}^+$ (**4**), $Y©B_6C_6^+$ (**5**), and $Sc©B_5C_6$ (**6**) at M06-2X level, with bond lengths indicated in Å.

3. Results and discussion

We start from LaC_{13}^+, the most concerned species observed in LaC_n^+ series (n = 12–40).[13] Encouragingly and interestingly, as shown in Fig. 1 and S1,† extensive GM searches indicate that LaC_{13}^+ possesses the well-defined perfect planar GM of D_{13h} $La©C_{13}^+$ (**1**) which contains a La atom located exactly at the center of the C_{13} wheel ligand, with the optimized La–C coordination bond lengths of $r_{La-C} = 2.70$ Å which are slightly longer than the sum of the self-consistent single-bond covalent radii of La and C (2.55 Å)[12] and C–C bond lengths of $r_{C-C} = 1.29$ Å which lie between C=C double-bond (1.34 Å) and C≡C triple bond (1.20 Å), setting up the highest coordination number of CN = 13 in planar species reported to date. $La©C_{13}^+$ (**1**) possesses the huge HOMO–LUMO gap of $\Delta E_{gap} = 5.33$ eV at M06-2X level, well underlying its high chemical stability. The slightly distorted triplet C_s LaC_{13}^+ ($^3A'$) appears to be the second lowest-lying isomer lying 2.41 eV above the GM at CCSD(T). The seventh C_{2v} isomer with a La inserted into the C_{13} ring and the fifth C_{2v} isomer with a La attached to the outside of the C_{13} ring are found to lie 3.36 eV and 3.09 eV higher in energy than the GM at M06-2X, respectively. Extensive BOMD simulations indicate that $La©C_{13}^+$ (**1**) is highly dynamically stable at both 800 K and 1000 K, with the small average root-mean-square-deviations of RMSD = 0.11 and 0.13 Å and maximum bond length deviations of MAXD = 0.31 and 0.36 Å, respectively (Fig. S7†). No high-lying isomers were observed during the dynamical simulations.

Replacing the La center in $La©C_{13}^+$ (**1**) with a Ca atom generates the charge-transfer neutral complex D_{13h} $Ca©C_{13}$ (**2**). The Ca center in $Ca©C_{13}$ (**2**) matches the C_{13} wheel ligand

perfectly both electronically and geometrically though it has a much lower Wiberg bond index of $WBI_{Ca} = 0.26$ than La in La©C_{13}^+ (**1**) where $WBI_{La} = 1.76$ (Table 1). The Ca–C coordination interaction with the low bond order of $WBI_{Ca-C} = 0.02$ in Ca^{2+}©C_{13}^{2-} (**2**) is thus almost purely ionic. Using an Ac atom which has a larger atomic radius than La to replace La in La©C_{13}^+ (**1**), the slightly buckled C_{13v} Ac©C_{13}^+ (**3**) is generated in which the Ac atom lies 0.59 Å above the C_{13} ring, with the periphery C–C distances of $r_{C-C} = 1.29$ Å remaining basically unchanged. The experimentally observed prominent ScC_{13}^+ and YC_{13}^+ monocations[15] have severely off-centered C_{2v} Sc©C_{13}^+ ($^1A_1$) (with CN = 8) and C_{2v} Y©C_{13}^+ ($^1A_1$) (with CN = 9) GM structures due to strong ring strains, respectively, while the open-shell CeC_{13}^+ possesses a slightly distorted GM C_{2v} Ce©C_{13}^+ ($^2B_2$) which has practically a D_{13h} symmetry (Fig. S8†). With one more valence electron detached, the Ce©C_{13}^{2+} dication isovalent with La©C_{13}^+ (**1**) has indeed a perfect D_{13h} GM (Fig. S8†).

It is natural to ask at current stage whether it is possible to form metal-centered monocyclic carbon wheel clusters with coordination numbers greater than thirteen (*i.e.*, CN > 13). We carefully checked the hypercoordination chemistry of the experimentally observed La©C_{14}^+ in this work. Although a bare C_{14} has a perfect C_{7h} acetylenic structure,[39] with a La atom added in, the La-doped LaC_{14}^+ possesses the off-centered planar GM of C_{2v} La©C_{14}^+ (**4**) which has the actual coordination number of CN = 11 (Fig. 1 and S4†). The three C atoms on the top part of La©C_{14}^+ (**4**) with La–C distances great than 3.1 Å have the practically negligible La–C coordination bond orders (with $WBI_{La-C} \approx 0.00$). Using Ac, the largest actinide metal in the periodical table, to replace La,[12] an elongated planar D_{2h} Ac©C_{14}^+ (Fig. S8†) with CN = 12 is generated. A C_{14} ring is obviously too big in size to host a transition-metal atom at its geometrical center comfortably to form a perfect wheel complex D_{nh} M©C_n with the same M–C coordination bonding distances. We conclude that CN = 13 is the highest coordination number in metal-centered monocyclic carbon wheel clusters M©C_n^+ with effective M–C coordination interactions.

Introducing certain numbers of B atoms into the carbon rings generates more structural diversities in B–C binary wheel ligands B_mC_n with CN ≤ 13. As examples, the metal-centered monocyclic C–B binary wheel complexes Y©$B_6C_6^+$ (**5**) and Sc©B_5C_6 (**6**) in Fig. 1 and C_{2v} La©BC_{12} in Fig. S8† as the GMs of the systems possess the coordination numbers of CN = 12, 11, and 13, respectively. These planar C–B binary wheel complexes have larger C–B and B–B periphery distances than the corresponding C–C distances in La©C_{13}^+ (**1**) because B has a larger covalent radius than C.

To interpret the high stabilities of these hypercoordinated planar species, we performed detailed NBO and molecular orbital analyses on La©C_{13}^+ (**1**), Y©$B_6C_6^+$ (**5**), and Sc©B_5C_6 (**6**). As tabulated in Table 1, the La center in La©C_{13}^+ (**1**) possesses the natural atomic charge of $q_{La} = +2.08$ |e|, electronic configuration of $La[Xe]4f^{0.43}5d^{0.41}6s^{0.02}$, and total Wiberg bond order of $WBI_{La} = 1.76$. The C atoms on the C_{13} wheel ligand have the total Wiberg bond orders of $WBI_C = 3.99$ and C–C bond orders of $WBI_{C-C} = 1.73$, revealing the cumulenic nature of the complex. Obviously, the La center donates its 6s electron almost completely to the C_{13} ligand. The La–C_{13} coordination

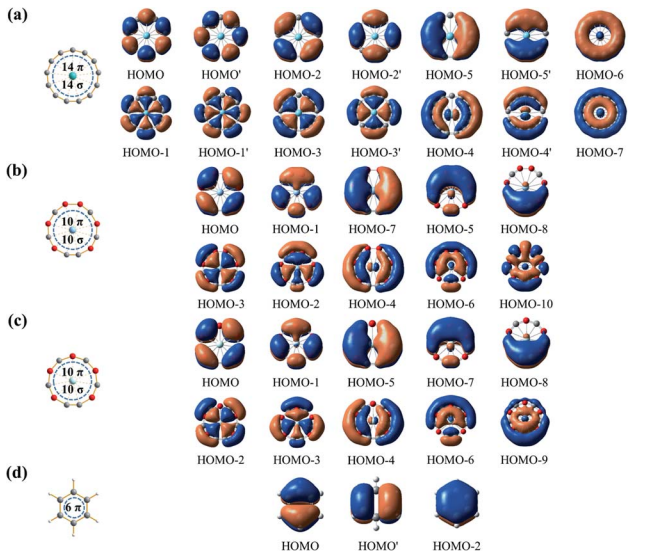

Fig. 2 Delocalized π- and σ-CMOs of (a) La©C_{13}^+ (**1**), (b) Y©$B_6C_6^+$ (**5**), and (c) Sc©B_5C_6 (**6**), in comparison with the delocalized π-CMOs of (d) D_{6h} C_6H_6.

Table 1 Calculated HOMO–LUMO gaps ΔE_{gap}/eV, natural atomic charges q_M, electronic configurations, and Wiberg bond indexes WBI_M of the metal centers M and Wiberg bond indexes of the M–C (WBI_{M-C}) and M–B (WBI_{M-B}) coordination interactions and NICS values 1.0 Å above the metal centers (NICS (1)) of the $M^{(x)}$©$B_mC_n^{k\pm}$ complex series (**1–6**) at M06-2X level

$M^{(x)}$©$B_mC_n^{k\pm}$	CN	ΔE_{gap}/eV	q_M	Electronic configurations of central metal M	WBI_M	WBI_{M-C}	WBI_{M-B}	NICS (1)
D_{13h} La©C_{13}^+ (**1**)	13	5.33	2.08	$[Xe]\ 4f^{0.43}5d^{0.41}6s^{0.02}$	1.76	0.14	—	−58.54
D_{13h} Ca©C_{13} (**2**)	13	5.63	1.87	$[Ar]\ 3d^{0.09}4s^{0.03}4p^{0.01}$	0.26	0.02	—	−44.68
C_{13v} Ac©C_{13}^+ (**3**)	13	5.26	2.38	$[Rn]\ 5f^{0.19}6d^{0.35}7s^{0.03}$	1.22	0.10	—	−55.16
C_{2v} La©C_{14}^+ (**4**)	11	3.72	2.15	$[Xe]\ 4f^{0.28}5d^{0.50}6s^{0.03}$	1.64	0.07–0.16	—	−29.21
C_{2v} Y©$B_6C_6^+$ (**5**)	12	5.70	2.12	$[Kr]\ 5s^{0.06}4d^{0.70}5p^{0.01}$	1.67	0.10–0.22	0.09–0.12	−24.08
C_{2v} Sc©B_5C_6 (**6**)	11	5.32	1.94	$[Ar]\ 3d^{0.87}4s^{0.07}4p^{0.02}$	1.94	0.13–0.29	0.13–0.14	−29.62

interactions mainly originate from contributions involving the 5d and 4f atomic orbitals of the La center, as indicated in the degenerated π-HOMO/HOMO′, π-HOMO-2/HOMO-2′, σ-HOMO-1/HOMO-1′, and σ-HOMO-3/HOMO-3 in Fig. 2(a). Although each La–C coordination interaction in La©C_{13}^+ (**1**) has a relatively low bond order (WBI_{La-C} = 0.14), the thirteen equivalent La–C coordination bonds function together to effectively stabilize the hypercoordinated cluster, making it the well-defined GM of the system observed solely in gas-phase experiments.[13,14] Similar situations happen in Ac©C_{13}^+ (**3**), Y©$B_6C_6^+$ (**5**), and Sc©B_5C_6 (**6**).

The 14 totally delocalized canonical molecular orbitals (CMOs) of La©C_{13}^+ (**1**) are collectively shown in Fig. 2(a), including 7 delocalized π-CMOs and 7 delocalized σ-CMOs. Its remaining 13 σ-CMOs correspond to 13 two-center-two-electron (2c-2e) C–C σ bonds along the periphery of the C_{13} ligand (Fig. S9†). The degenerate f-type HOMO/HOMO′, d-type HOMO-2/HOMO-2′ and p-type HOMO-5/HOMO-5′ and non-degenerate s-type HOMO-6 possess three, two, one, and zero nodal surfaces, respectively, forming an out-of-plane 14 π electron system matching the $4N_\pi + 2$ aromatic rule with $N_\pi = 3$. Similarly, the degenerate HOMO-1/HOMO-1′, HOMO-3/HOMO-3′, and HOMO-4/HOMO-4′ and non-degenerate HOMO-7 form an in-plane 14 σ electron system matching the $4N_\sigma + 2$ aromatic rule with $N_\sigma = 3$. Such a unique 14 σ + 14 π electronic configuration renders σ + π dual aromaticity to La©C_{13}^+ (**1**), effectively stabilizing the monocation observed in experiments, similar to the situation in the σ + π dually aromatic D_{10h} Ta©B_{10}^- which possesses a 10 σ + 6 π electronic configuration.[1] It is noticed that metal-centered wheel D_{13h} La©C_{13}^+ (**1**) has the same numbers of delocalized σ and π electrons (14 σ + 14 π) as the highly stable ring-like acetylenic C_{7h} C_{14}.[39]

As shown in Fig. 2(b) and (c), both the metal-centered monocyclic C–B binary wheel clusters Y©$B_6C_6^+$ (**5**) and Sc©B_5C_6 (**6**) have 5 delocalized π-CMOs and 5 delocalized σ-CMOs, forming an out-of-plane 10 π electron system conforming to the $4N_\pi + 2$ π-aromatic rule ($N_\pi = 2$) and an in-plane 10 σ electron system conforming to $4N_\sigma + 2$ σ aromatic rule ($N_\sigma = 2$). Such 10 σ + 10 π electronic configurations make both Y©$B_6C_6^+$ (**5**) and Sc©B_5C_6 (**6**) σ + π dually aromatic in nature, similar to but with more delocalized electrons than the previously reported Co©B_8^- and Ru©B_9^- with 6 σ + 6 π delocalized electrons and Ta©B_{10}^- and Nb©B_{10}^- with 10 σ + 6 π delocalized electrons.[1,5–8]

The La–C_{13} coordination interactions in La©C_{13}^+ (**1**) mainly originate from d–p and f–p σ-coordination interactions involving the in-plane La $5d_{x^2-y^2}/5d_{xy}$ and $4f_{x(x^2-3y^2)}/4f_{y(y^2-3x^2)}$ atomic orbitals and C $2p_x/2p_y$ hybridized atomic orbitals, as demonstrated in the degenerated HOMO-3/HOMO-3′ (5d–2p σ-coordination) and HOMO-1/HOMO-1′ (4f–2p σ-coordination) in Fig. 2(a), respectively. Quantitatively, the La center contributes more to the delocalized in-plane σ-CMOs (2.81–7.63%) than to the delocalized out-of-plane π-CMOs (0.08–3.66%). The delocalized in-plane σ-CMOs thus dominate the La–C coordination bonding interactions. Similarly, the in-plane 4d–2p σ-coordination interactions (HOMO-2 and HOMO-3) in Y©$B_6C_6^+$ (**5**) and 3d–2p σ-coordination interactions (HOMO-2 and HOMO-3) in Sc©B_5C_6 (**6**) dominate the metal–ligand interactions in the two 10 σ + 10 π systems.

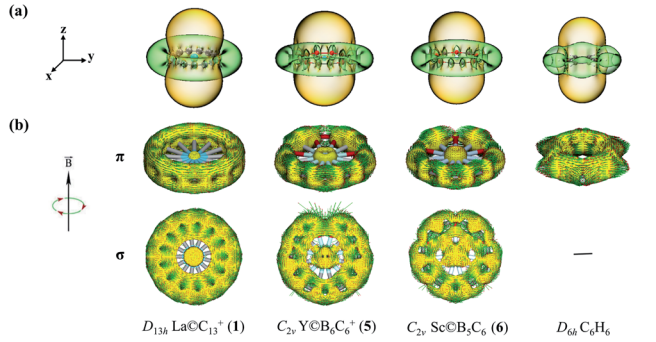

Fig. 3 (a) Calculated iso-chemical shielding surfaces (ICSSs) of La©C_{13}^+ (**1**), Y©$B_6C_6^+$ (**5**), and Sc©B_5C_6 (**6**), compared with that of aromatic benzene C_6H_6. Yellow and green regions stand for chemical shielding and de-shielding areas, respectively. (b) Calculated π- and σ-ring current maps of La©C_{13}^+ (**1**), Y©$B_6C_6^+$ (**5**), and Sc©B_5C_6 (**6**), respectively, in comparison with the π-ring current map of D_{6h} C_6H_6. The external magnetic field is perpendicular to the wheel plane. The red arrows represent directions and magnitudes of the ring currents at various positions on the ACID iso-surfaces.

The aromatic nature of La©C_{13}^+ (**1**), Y©$B_6C_6^+$ (**5**), and Sc©B_5C_6 (**6**) is further evidenced by their calculated nucleus-independent chemical shift (NICS) values. Based on the calculated NICS-ZZ components, Fig. 3(a) depicts the ICSS surfaces of **1**, **5**, and **6** with the *Z*-axis perpendicular to the molecular planes to illuminate the chemical shielding around the metal centers, in comparison with that of the prototypical aromatic benzene (C_6H_6). Obviously, the space inside the C_{13}, B_6C_6, or B_5C_6 rings in horizontal direction or within about 1.0 Å above the metal centers in vertical direction belong to chemical shielding regions with negative NICS-ZZ values (highlighted in yellow), while the chemical de-shielding areas with positive NICS values (highlighted in green) are located outside the wheel ligands in horizontal direction. Fig. 3(a) clearly shows the ICSS surfaces of these metal-centered planar complexes are exactly similar to that of the aromatic benzene.

Calculating the anisotropy of current-induced density (ACID)[34] is an effective approach to graphically display the ring currents induced by an external magnetic field in vertical directions perpendicular to the molecular planes. ACID can be decomposed into σ and π components separately. Fig. 3(b) clearly indicates the π-ring current maps of La©C_{13}^+ (**1**), Y©$B_6C_6^+$ (**5**), and Sc©B_5C_6 (**6**) are extremely similar to the corresponding π-ring current map of π-aromatic benzene C_6H_6. Besides, in contrast to benzene which possesses no delocalized σ-electrons, La©C_{13}^+ (**1**), Y©$B_6C_6^+$ (**5**), and Sc©B_5C_6 (**6**) also exhibit strong σ-ring currents, rendering additional σ-aromaticity to stabilize the systems, as shown in Fig. 3(b) (see Fig. S10† for high-resolution π- and σ-ring current maps of **1**, **5**, and **6**). The observation of both σ- and π-diatropic ring currents in **1**, **5**, and **6** well supports the σ + π dually aromatic nature of these planar hypercoordinated complexes.

Based on the planar hypercoordinated species discussed above, we develop a universal electronic design principle for σ +

π dually aromatic metal-centered monocyclic boron, carbon, or boron-carbon binary wheel clusters $M^{(x)}©B_mC_n^{k\pm}$. There exist $m + n$ 2c-2e σ bonds along the periphery of the monocyclic B_mC_n wheel ligand. With each C atom providing two delocalized electrons and each B atom contributing one delocalized electron, the total number of the delocalized electrons in $M^{(x)}©B_mC_n^{k\pm}$ matches the requirement of σ + π dual aromaticity of the system:

$$m + 2n + x \pm k = L \ (L = 12, 16, 20, \text{or } 28) \quad (1)$$

where L is the total number of delocalized σ and π electrons each matching the $4N + 2$ rule and x stands for the formal valence of the central atom M. Such an electronic design principle covers the previously observed D_{7h} B©B_7^{2-}, D_{8h} B©B_8^-, D_{9h} Co©B_8^-, and D_{9h} Ru©B_9^- where $L = 12$ and $x = 3$, 3, 3, and 2 and D_{10h} Ta©B_{10}^- and D_{10h} Nb©B_{10}^- where $L = 16$ and $x = 5$ and 5, respectively. For the currently discussed La©C_{13}^+ (**1**), Ca©C_{13} (**2**), and Ac©C_{13}^+ (**3**), $L = 28$ and $x = 3$, 2, and 3, while for Y©$B_6C_6^+$ (**5**) and Sc©B_5C_6 (**6**), $L = 20$ and $x = 3$ and 3, respectively. The slightly buckled C_{13v} Ac©C_{13}^+ (**3**) follows the same electronic design principle though the Ac center in it slightly mismatches the C_{13} wheel ligand in geometry. Eqn (1) can be easily extended to σ + π dually aromatic B–C–N ternary wheel complexes $M^{(x)}©B_mC_nN_l^{k\pm}$ where it reads: $m + 2n + 3l + x \pm k = 28$, as demonstrated in the cases of C_s La©BNC_{11}^+ and C_s La©$B_4N_4C_5^+$ (Fig. S8†) in which each N atom contributes three valence electrons to the delocalized systems. However, extensive test calculations indicate that inclusion B or N atoms in the wheel ligands does not help to improve the maximum coordination numbers of the systems.

The highly stable La©C_{13}^+ (**1**) with a wide HOMO–LUMO gap and fully occupied bonding inner-shell CMOs can be used as a super-hydrogen monocation (H^+) to form various substituted multi-nuclei complexes. Typical examples include C_{13v} [La©C_{13}]X (X = F, Cl, Br) (**7**), D_{13h} [La©C_{13}]$^+L_2$ (L = Ar, Kr) (**8**), C_{2v} [La©C_{13}]$_2$O (**9**), and C_{3v} N[La©C_{13}]$_3$ (**10**) (Fig. 4) which can be derived from the parent species $C_{\infty v}$ HX, $D_{\infty h}$ H^+L_2, C_{2v} H_2O, and C_{3v} NH_3 by substituting H^+ monocation(s) with La©C_{13}^+ (**1**) unit(s), respectively, presenting the viable possibility to form complex compounds with multiple hypercoordinated metal centers.

Finally, as examples, the simulated IR, Raman, and UV-vis spectra of D_{13h} La©C_{13}^+ (**1**) and C_{2v} Y©$B_6C_6^+$ (**5**) are presented in Fig. S11† to facilitate their spectroscopic characterizations. La©C_{13}^+ (**1**) possesses highly simplified spectra due to its perfect D_{13h} symmetry. It has two main IR peaks at 39 (a_2'') and 866 (e_1') cm^{-1}, three Raman peaks at 272 (e_2'), 664 (a_1'), and 1280 (e_2') cm^{-1}, and three UV absorption peaks at 156 (A_1'), 174 (E_2'), and 200 (E_2') nm, respectively. C_{2v} Y©$B_6C_6^+$ (**5**) has more complicated spectra, with two main IR absorption peaks at 499 (b_1) and 588 (b_2) cm^{-1}, two major Raman scattering bands at 211 (b_2) and 623 (a_1) cm^{-1}, and five UV absorption bands around 134 ($^1B_2$), 161 ($^1A_1$), 191 ($^1B_2$), 207 ($^1A_1$), and 219 ($^1B_2$) nm, respectively.

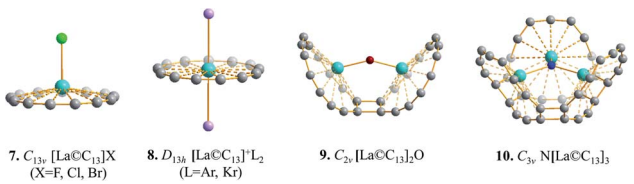

Fig. 4 Optimized structures of [La©C_{13}]X (**7**) (X = F, Cl, Br), [La©C_{13}]$^+L_2$ (**8**) (L = Ar, Kr), [La©C_{13}]$_2$O (**9**), and N[La©C_{13}]$_3$ (**10**) at M06-2X level.

4. Conclusions

Extensive first-principles theory calculations performed in this work unveil the highest coordination numbers of CN = 13 in La©C_{13}^+ (**1**), Ca©C_{13} (**2**), and Ac©C_{13}^+ (**3**), CN = 12 in Y©$B_6C_6^+$ (**5**), and CN = 11 in La©C_{14}^+ (**4**) and Sc©B_5C_6 (**6**) reported to date in planar species, effectively enriching the structural and bonding patterns in planar hypercoordination chemistry. σ + π dually aromatic metal-centered monocyclic B–C binary wheel complexes $M^{(x)}©B_mC_n^{k\pm}$ follow the electronic design principle of $m + 2n + x \pm k = L$ ($L = 12$, 16, 20, or 28) which can be readily extended to more complicated systems containing other periphery atoms rather than B and C. The recent experimental identification of the sp-hybridized molecular carbon allotrope, π-aromatic C_{18}, induced by atom manipulations,[9] presents the possibility to synthesize and characterize the σ + π dually aromatic La©C_{13}^+ (**1**) and its complex compounds to open a new area in planar hypercoordination chemistry, catalysis, and materials science.

Conflicts of interest

There are no conflicts to declare.

Acknowledgements

The work was supported by the National Natural Science Foundation of China (21720102006 and 21973057 to S.-D. Li).

Notes and references

1 T. R. Galeev, C. Romanescu, W. L. Li, L. S. Wang and A. I. Boldyrev, *Angew. Chem., Int. Ed.*, 2012, **51**, 2101–2105.
2 T. Heine and G. Merino, *Angew. Chem., Int. Ed.*, 2012, **51**, 4275–4276.
3 H. J. Zhai, A. N. Alexandrova, K. A. Birch, A. I. Boldyrev and L. S. Wang, *Angew. Chem., Int. Ed.*, 2003, **42**, 6004–6008.
4 C. Romanescu, T. R. Galeev, W. L. Li, A. I. Boldyrev and L. S. Wang, *Angew. Chem., Int. Ed.*, 2011, **123**, 9506–9509.
5 C. Romanescu, T. R. Galeev, W. L. Li, A. I. Boldyrev and L. S. Wang, *Angew. Chem., Int. Ed.*, 2011, **50**, 9334–9337.
6 C. Romanescu, T. R. Galeev, W. L. Li, A. I. Boldyrev and L. S. Wang, *Acc. Chem. Res.*, 2013, **46**, 350–358.
7 C. Romanescu, T. R. Galeev, W. L. Li, A. I. Boldyrev and L. S. Wang, *J. Chem. Phys.*, 2013, **138**, 134315.
8 W. L. Li, C. Romanescu, T. R. Galeev, Z. A. Piazza, A. I. Boldyrev and L. S. Wang, *J. Am. Chem. Soc.*, 2012, **134**, 165–168.

9 K. Kaiser, L. M. Scriven, F. Schulz, P. Gawel, L. Gross and H. L. Anderson, *Science*, 2019, **365**, 1299–1301.
10 Z. Liu, X. Wang, T. Lu, A. Yuan and X. Yan, *ChemRxiv*, 2021, DOI: 10.26434/chemrxiv.14601168.v1.
11 Y. Jiang, Y. Wu, J. Deng and Z. Wang, *Phys. Chem. Chem. Phys.*, 2021, **23**, 8817–8824.
12 P. Pyykkç and M. Atsumi, *Chem.–Eur. J.*, 2009, **15**, 12770–12779.
13 D. E. Clemmer, K. B. Shelimov and M. F. Jarrold, *J. Am. Chem. Soc.*, 1994, **116**, 5971–5972.
14 K. B. Shelimov, D. E. Clemmer and M. F. Jarrold, *J. Phys. Chem.*, 1995, **99**, 11376–11386.
15 R. Klingeler, P. S. Bechthold, M. Neeb and W. Eberhardt, *J. Chem. Phys.*, 2000, **113**, 4.
16 S. Roszak and K. Balasubramanian, *Chem. Phys. Lett.*, 1997, **264**, 80–84.
17 D. L. Strout and M. B. Hall, *J. Phys. Chem. A*, 1998, **102**, 641–645.
18 X. Chen, Y. F. Zhao, Y. Y. Zhang and J. Li, *J. Comput. Chem.*, 2019, **40**, 1105–1112.
19 D. J. Wales and H. A. Scheraga, *Science*, 1999, **285**, 1368–1372.
20 J. P. Perdew, K. Burke and M. Ernzerhof, *Phys. Rev. Lett.*, 1996, 77, 3865.
21 J. VandeVondele, M. Krack, F. Mohamed, M. Parrinello, T. Chassaing and J. Hutter, *Comput. Phys. Commun.*, 2005, **167**, 103–128.
22 Y. Zhao and D. G. Truhlar, *Theor. Chem. Acc.*, 2008, **120**, 215–241.
23 C. Adamo and V. Barone, *J. Chem. Phys.*, 1999, **110**, 6158–6170.
24 R. Krishnan, J. S. Binkley, R. Seeger and J. A. Pople, *J. Chem. Phys.*, 1980, **72**, 650–654.
25 D. Feller, *J. Comput. Chem.*, 1996, **17**, 1571–1586.
26 L. Schuchardt, B. T. Didier, T. Elsethagen, L. Sun, V. Gurumoorthi, J. Chase, J. Li and T. L. Windus, *J. Chem. Inf. Model.*, 2007, **47**, 1045–1052.
27 M. J. Frisch, *et al.*, *Gaussian 16, Revision A.03*, Gaussian Inc., Wallingford, CT, 2016.
28 J. Čížek, *Adv. Chem. Phys.*, 1969, **14**, 35.
29 G. D. Purvis III and R. J. Bartlett, *J. Chem. Phys.*, 1982, **76**, 1910.
30 K. Raghavachari, G. W. Trucks, J. A. Pople and M. Head-Gordon, *Chem. Phys. Lett.*, 1989, **157**, 479–483.
31 H. J. Werner, *et al.*, *Molpro, version.1.*, 2012, (www.molpro.net).
32 P. E. D. Glendening, J. K. Badenhoop, A. E. Reed, J. E. Carpenter, J. A. Bohmann, C. M. Morales, C. R. Landis and F. Weinhold, *NBO 6.0*, 2013.
33 D. Geuenich, K. Hess, F. Köhler and R. Herges, *Chem. Rev.*, 2005, **105**, 3758–3772.
34 Povray, Persistence of vision raytracer, *POV-Ray 3.7*, http://www.povray.org.
35 S. Klod and E. Kleinpeter, *J. Chem. Soc., Perkin Trans. 2*, 2001, **2**, 1893–1898.
36 E. Kleinpeter, S. Klod and A. Koch, *J. Mol. Struct.*, 2007, **811**, 45–60.
37 T. Lu and F. W. Chen, *J. Comput. Chem.*, 2012, **33**, 580–592.
38 R. Bauernschmitt and R. Ahlrichs, *Chem. Phys. Lett.*, 1996, **256**, 454–464.
39 S. Arulmozhiraja and T. Ohno, *J. Chem. Phys.*, 2008, **128**, 114301.